CONEM 2022
CONGRESSO NACIONAL DE ENGENHARIA MECÂNICA
TERESINA - PI

ABCM

XI CONGRESSO NACIONAL DE ENGENHARIA MECÂNICA
DE 07 A 11 DE AGOSTO DE 2022, TERESINA-PI, BRASIL

# ON THE COUPLING OF A ONE-DIMENSIONAL PERIODIC STRUCTURE TO A BEAM HOST STRUCTURE

**Vinícius Mauro de Souza Santos, engviniciusouza@gmail.com**[1]
**Thiago de Paula Sales, tpsales@ita.br**[1]

[1]Instituto Tecnológico de Aeronáutica

***Abstract:*** *Phononic crystals (PCs) and locally resonant periodic structures have been intensively studied lately, as they can provide a means for vibration attenuation. This is due to their underlying dynamic behavior, which is characterized by frequency ranges on which wave propagation is entirely evanescent, which are known as bandgaps. These can be used to achieve vibration isolation, as well as to enable localized modes, when one defect is introduced on the periodic lattice, for example. On the other hand, there remains the question if periodic structure behavior can be leveraged for structures which already exist, i.e., is it possible to couple a periodic structure appendage to an existing structure so the latter is able to benefit from bandgaps on the former? To investigate this matter, in this work one considers the coupling of a one-dimensional periodic structure (1D-PS), whose unit cell can be arbitrary, which is attached "in parallel" to a beam host structure (HS). The former can be either a "conventional structure", a PC, or even a metastructure (MS). To model the dynamic behavior of the 1D-PS, the wave-based finite element method (WFEM) is employed. A strategy is presented to duly account for non-periodicities which ensue due to coupling on particular unit cells of the waveguide. To model the dynamic behavior of the HS, one employs the spectral element method (SEM). The coupling between the 1D-PS and the HS is modeled by lumped, discrete spring elements. To account for their influence, the WFEM and SEM equations are suitably modified. Numerical simulations are performed in MATLAB®, enabling us to obtain dispersion relations for "coupled" and "uncoupled" unit cells, and to assess the dynamics of the coupled system. Traditional finite element analysis (FEA) is also performed in order to validate in-house implemented codes, as well as the proposed modeling strategy. Longitudinal and bending behaviors are investigated separately for the considered system. In these settings, one also assesses the influence of the value of the coupling spring stiffness, which is taken to be soft or hard. It is seen that the proposed strategy for modeling the coupled system behavior is adequate. Additionally, due to the underlying characteristics of the WFEM, it has been observed that a large number of wave modes needs to be taken into account to properly represent responses.*
***Key words:*** *periodic structures, coupling, WFEM, SEM, FEA*

## 1. INTRODUCTION

Some periodic structures have attracted attention in the last decades due to their unusual behavior. When it comes to mechanical waves, attenuation of acoustic waves and vibrations are of interest in several practical applications. Great reviews regarding the dynamic behavior of periodic structures are available (Hussein *et al.*, 2014; Banerjee *et al.*, 2019; Muhammad and Lim, 2022), which discuss some of their fundamental aspects, such as the concepts of bandgap, phononic crystal, resonant metastructure, etc. In particular, a metastructure (MS) can be interpreted as a periodic structure whose behavior is different from those exhibited by "conventional structures". It can possess bandgaps, i.e. frequency ranges in which wave propagation is purely evanescent, which can arise due to Bragg scattering or periodically-arranged local resonators, for example. Within this context, Mizukami *et al.* (2021) have shown that bandgap width, structure stiffness and weight can be improved by using continuous carbon-fiber-reinforced plastics in MS which exploit inertial amplification mechanisms.

When a MS is coupled to an already existing "conventional structure", as in the case depicted in Fig. 1, a fundamental question arises, related to the dynamic behavior of the coupled system. Does or can the "conventional" host structure (HS) benefit from unusual properties exhibited by the MS? This is very important, for enabling one to assess if MS attachments can be effective for reducing vibration of a given HS. Of course, coupled systems have been thoroughly investigated in the literature. For example, in a recent related work, the dynamic behavior of beams which are coupled through resonators has been investigated by He *et al.* (2022).

If one wants to analyze the dynamic behavior of a MS, then we might resort to the wave-based finite element method (WFEM) (Hoang *et al.*, 2020), that is an efficient numerical tool for modeling periodic structures based on their unit cell's wave propagation characteristics. According to Mencik (2014), the WFEM enables a large decrease of computational

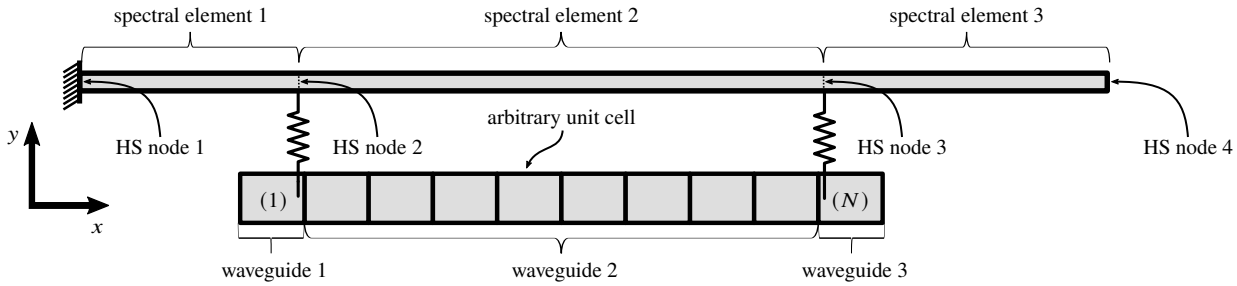


Figure 1: **A clamped-free beam host structure coupled by springs to a periodic structure with $N$ unit cells.**

time when compared to the traditional FEM, due to the reduced size of matrices found in the wave propagation-based approach. Essentially, in the WFEM, one uses traditional FEM to model the dynamic behavior of the unit cell of the periodic structure. Based on the Bloch-Floquet theorem, and on the FEM-provided dynamic stiffness matrix, it is possible to determine eigenvalues and eigenvectors (wave-modes) related to wave propagation. These can afterward be used to compute forced responses of a finite periodic structure, by relying on wave-mode based expansion representations (Mencik and Duhamel, 2015). In various studies, the WFEM has been used to address the modeling of periodic structures which do not possess "defects", or that are not coupled to other waveguides via elastic joints (Duhamel *et al.*, 2006; Waki *et al.*, 2009b; Mencik, 2010; Hoang *et al.*, 2020). On the other hand, some studies have also tackled such cases (Silva *et al.*, 2016; Vivien and Mencik, 2020).

Concerning the dynamic behavior of a HS, such as the clamped-free beam seen in Fig. 1, we can adopt the spectral element method (SEM) as a frequency domain modeling strategy (Lee, 2009). The use of the SEM in this setting is justified due to the non-complex geometry assumed for the HS, i.e. a slender straight beam with, say, a rectangular cross-section. For this type of HS, an exact solution is possible for its equations of motion, based on wave propagation. Within the context of the SEM, the use of a single finite spectral element between discontinuities enables one to obtain the exact solution foreseen by the underlying mechanical theory, such as Timoshenko beam theory in the considered case. This occurs because frequency-dependent shape functions are adopted in the method. As a result, a small number of elements need to be used when the SEM strategy is adopted.

It is challenging, on the other hand, to model the dynamic behavior of the coupled system presented in Fig. 1 when considering the WFEM to model the MS, and the SEM to model the HS. To the best of the authors' knowledge, combining both of these modeling methods in the alluded scenario has not been investigated. To perform this task here, only a rather simple coupling between the MS and HS is considered, assumed as being properly described by lumped, discrete spring elements. The coupling, on its hand, breaks the perfect periodicity of the MS, which leads to difficulties in the application of the WFEM – which can not be used without proper amendments. Thus, a strategy must be employed to circumvent this issue, which consists of an objective of the present work.

In this article, we initially present the equations related to the SEM and WFEM methodologies, and later take into account the coupling which can happen between HS and MS by lumped, discrete springs, cf. Fig. 1. The proposed methodology is validated by comparing a considerable number of frequency response functions (FRFs) obtained through our implement codes and from commercial finite element software. Longitudinal and bending behaviors are investigated considering soft and hard coupling springs.

## 2. MODELING

In this section, we first provide brief reviews of the SEM (for a two-dimensional beam) and the WFEM modeling strategies. Afterwards, the methodology adopted for coupling both of these methods, due to the springs which couple the HS and MS, is considered.

### 2.1. Spectral Element Method Considering the Extended Timoshenko Beam Theory

The spectral element for the extended Timoshenko beam (ETB) theory has two nodes, and three degrees of freedom (DOFs) per node, related to axial ($U$) and transverse ($V$) displacements, and slope ($\Theta$). The loads associated to each of these DOFs are the axial tensile force, the transverse shear force and the bending moment, denoted $N$, $Q$ and $M$, respectively. Relevant geometric and material parameters of the beam are: its length, $L$; its cross-sectional area, $A$; the longitudinal and shear moduli, $E$ and $G$; the mass density per unit volume, $\rho$; the shear correction factor, $\kappa$; the static moment of area, $R$; the area moment of inertia about the neutral axis, $I$; and the coupling rigidities between axial, transverse shear and bending

deformations, $C_1$, $C_2$ and $C_3$. The governing equations in the frequency domain of the ETB are (Lee, 2009):

$$\begin{bmatrix} EA & C_1 & C_2 \\ C_1 & \kappa GA & C_3 \\ C_2 & C_3 & EI \end{bmatrix} \begin{Bmatrix} U'' \\ V'' \\ \Theta'' \end{Bmatrix} + \begin{bmatrix} 0 & 0 & -C_1 \\ 0 & 0 & -\kappa GA \\ C_1 & \kappa GA & 0 \end{bmatrix} \begin{Bmatrix} U' \\ V' \\ \Theta' \end{Bmatrix} - \begin{bmatrix} 0 & 0 & 0 \\ 0 & 0 & 0 \\ 0 & 0 & \kappa GA \end{bmatrix} \begin{Bmatrix} U \\ V \\ \Theta \end{Bmatrix} + \omega^2 \begin{bmatrix} \rho A & 0 & \rho R \\ 0 & \rho A & 0 \\ \rho R & 0 & \rho I \end{bmatrix} \begin{Bmatrix} U \\ V \\ \Theta \end{Bmatrix} = \begin{Bmatrix} 0 \\ 0 \\ 0 \end{Bmatrix}, \quad (1)$$

where the prime $(\,)'$ denotes differentiation w.r.t. the spatial coordinate and $\omega$ is the angular frequency.

Assuming $R$, $C_1$, $C_2$ and $C_3$ are equal to zero, one recovers decoupled equations of motion for the Timoshenko beam and axial rod. Additionally, taking $U = U_0 e^{-\mathrm{i}kx}$, $V = V_0 e^{-\mathrm{i}kx}$ and $\Theta = \Theta_0 e^{-\mathrm{i}kx}$, being i the imaginary unit, $x$ the coordinate along the axis of the beam, and $U_0$, $V_0$ and $\Theta_0$ arbitrary amplitudes, we can obtain, from Eq. (1), an eigenproblem for the wavenumber $k$. The resulting characteristic equation provides $k_1 = -k_2 = \omega\sqrt{\rho/E}$, $k_3 = -k_4 = \frac{1}{c}\sqrt{\frac{a+b}{2\sqrt{I}}}$ and $k_5 = -k_6 = \frac{1}{c}\sqrt{\frac{-a+b}{2\sqrt{I}}}$, with:

$$a = \omega\sqrt{I\rho^2E^2\omega^2 + 4\rho AEG^2\kappa^2 - 2I\rho^2EG\kappa\omega^2 + I\rho^2G^2\kappa^2\omega^2}, \qquad b = E\sqrt{I}\omega^2\rho + G\sqrt{I}\kappa\omega^2\rho, \qquad c = \sqrt{EG\kappa}.$$

Note that $k_1 = -k_2$ are wavenumbers related to longitudinal behavior, while the other ones concern bending. Based on the wavenumbers and corresponding modal ratios $\gamma_m = \Theta_{0m}/V_{0m}$ $(m = 3, ..., 6)$, one can express the beam internal loads as follows (Lee, 2009):

$$\begin{Bmatrix} N \\ Q \\ M \end{Bmatrix} = \begin{bmatrix} EA & 0 & 0 \\ 0 & \kappa GA & 0 \\ 0 & 0 & EI \end{bmatrix} \begin{Bmatrix} U' \\ V' - \Theta \\ \Theta' \end{Bmatrix} = \begin{bmatrix} EA & 0 & 0 \\ 0 & \kappa GA & 0 \\ 0 & 0 & EI \end{bmatrix} \begin{bmatrix} \mathbf{e}'\mathbf{E}^{-1} \\ \mathbf{e}'_V\mathbf{E}^{-1} - \mathbf{e}_\Theta\mathbf{E}^{-1} \\ \mathbf{e}'_\Theta\mathbf{E}^{-1} \end{bmatrix} \mathbf{p} = \mathbf{M}_1\mathbf{M}_2\mathbf{p}, \quad (2)$$

where $\mathbf{p} = \{U(0) \quad V(0) \quad \Theta(0) \quad U(L) \quad V(L) \quad \Theta(L)\}^{\mathrm{T}}$ and:

$$\mathbf{e} = \begin{bmatrix} e^{-\mathrm{i}k_1x} & e^{-\mathrm{i}k_2x} & 0 & 0 & 0 & 0 \end{bmatrix}, \qquad \mathbf{e}_V = \begin{bmatrix} 0 & 0 & e^{-\mathrm{i}k_3x} & e^{-\mathrm{i}k_4x} & e^{-\mathrm{i}k_5x} & e^{-\mathrm{i}k_6x} \end{bmatrix},$$
$$\mathbf{e}_\Theta = \mathbf{e}_V \,\mathrm{diag}\,(0, 0, \gamma_3, \gamma_4, \gamma_5, \gamma_6), \qquad \mathbf{E} = \begin{bmatrix} \mathbf{e}(0) & \mathbf{e}_V(0) & \mathbf{e}_\Theta(0) & \mathbf{e}(L) & \mathbf{e}_V(L) & \mathbf{e}_\Theta(L) \end{bmatrix}^{\mathrm{T}}.$$

By enforcing equilibrium at the boundaries of the ETB element, we can establish dynamic equilibrium, i.e. $\mathbf{H}^{(e)}\mathbf{p}^{(e)} = \mathbf{f}^{(e)}$, where the superscript $(e)$ is used to highlight quantities at the element level. Moreover:

$$\mathbf{H}^{(e)} = \begin{bmatrix} \mathbf{M}_1\mathbf{M}_2|_{x=0} \\ \mathbf{M}_1\mathbf{M}_2|_{x=L} \end{bmatrix} \quad \text{and} \quad \mathbf{f}^{(e)} = \begin{Bmatrix} -N(0) & -Q(0) & -M(0) & N(L) & Q(L) & M(L) \end{Bmatrix}^{\mathrm{T}} \quad (3)$$

are the dynamic stiffness matrix and the load vector for the decoupled ETB beam element, respectively. Traditional FEM procedures (based on DOF connectivity) can be used to establish dynamic equilibrium at the global level, i.e. $\mathbf{H}^{(g)}\mathbf{p}^{(g)} = \mathbf{f}^{(g)}$, where the superscript $(g)$ is used to denote global quantities.

### 2.2. The Wave-based Finite Element Method

The presentation given here for the WFEM is essentially a summary of the works of Hoang *et al.* (2020) and Mencik and Duhamel (2015).

#### 2.2.1. Basic Development

Consider a periodic structure formed by $N$ unit cells, as shown in Fig. 2. For a unit cell which is modeled by the traditional FEM, the DOF and load vectors can be partitioned according to their location being left, right or internal. These partitions are denoted, respectively, by $\mathbf{q}_j$ and $\mathbf{F}_j$, for $j \in \{L, R, I\}$.

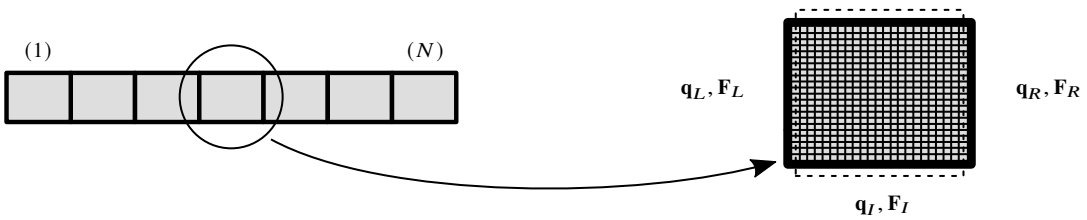


Figure 2: **Periodic structure containing $N$ unit cells.**

The equations of motion for the highlighted unit cell can be expressed as $\hat{\mathbf{M}}\ddot{\hat{\mathbf{q}}} + \hat{\mathbf{C}}\dot{\hat{\mathbf{q}}} + \hat{\mathbf{K}}\hat{\mathbf{q}} = \hat{\mathbf{f}}$, where $\hat{\mathbf{M}}$, $\hat{\mathbf{C}}$ and $\hat{\mathbf{K}}$ are the matrices of mass, damping and stiffness, respectively, $\hat{\mathbf{f}}$ is the load vector, $\ddot{\hat{\mathbf{q}}}$, $\dot{\hat{\mathbf{q}}}$ and $\hat{\mathbf{q}}$ are the acceleration, velocity and displacement vectors. Since the unit cell may contain many internal DOFs, the Craig-Bamptom (CB) method can be considered to obtain a reduced model, which can be written as $\mathbf{M}\ddot{\mathbf{q}}+\mathbf{C}\dot{\mathbf{q}}+\mathbf{K}\mathbf{q} = \mathbf{f}$, where $\hat{\mathbf{q}} = \boldsymbol{\alpha}\mathbf{q}$ has been used, $\boldsymbol{\alpha}$ denoting the CB projection matrix. Such procedure has also been adopted by Mencik (2018) and Zhou *et al.* (2015), for example.

In the frequency domain, we can write $\mathbf{D}\mathbf{q} = \mathbf{F}$, where $\mathbf{D} = -\omega^2\mathbf{M} + \mathrm{i}\omega\mathbf{C} + \mathbf{K}$ is the dynamic stiffness matrix. Segregating the DOFs and nodal loads according to the previously mentioned partition, we can write:

$$\begin{bmatrix} \tilde{\mathbf{D}}_{LL} & \tilde{\mathbf{D}}_{LR} & \tilde{\mathbf{D}}_{LI} \\ \tilde{\mathbf{D}}_{RL} & \tilde{\mathbf{D}}_{RR} & \tilde{\mathbf{D}}_{RI} \\ \tilde{\mathbf{D}}_{IL} & \tilde{\mathbf{D}}_{IR} & \tilde{\mathbf{D}}_{II} \end{bmatrix} \begin{Bmatrix} \mathbf{q}_L \\ \mathbf{q}_R \\ \mathbf{q}_I \end{Bmatrix} = \begin{Bmatrix} \mathbf{F}_L \\ \mathbf{F}_R \\ \mathbf{F}_I \end{Bmatrix} \quad \Rightarrow \quad \begin{bmatrix} \mathbf{D}_{LI}\mathbf{F}_I \\ \mathbf{D}_{RI}\mathbf{F}_I \end{bmatrix} + \begin{bmatrix} \mathbf{D}_{LL} & \mathbf{D}_{LR} \\ \mathbf{D}_{RL} & \mathbf{D}_{RR} \end{bmatrix} \begin{Bmatrix} \mathbf{q}_L \\ \mathbf{q}_R \end{Bmatrix} = \begin{Bmatrix} \mathbf{F}_L \\ \mathbf{F}_R \end{Bmatrix}, \tag{4}$$

where:

$$\mathbf{D}_{LI} = \tilde{\mathbf{D}}_{LI}\tilde{\mathbf{D}}_{II}^{-1}, \qquad \mathbf{D}_{LL} = \tilde{\mathbf{D}}_{LL} - \tilde{\mathbf{D}}_{LI}\tilde{\mathbf{D}}_{II}^{-1}\tilde{\mathbf{D}}_{IL}, \qquad \mathbf{D}_{LR} = \tilde{\mathbf{D}}_{LR} - \tilde{\mathbf{D}}_{LI}\tilde{\mathbf{D}}_{II}^{-1}\tilde{\mathbf{D}}_{IR},$$
$$\mathbf{D}_{RI} = \tilde{\mathbf{D}}_{RI}\tilde{\mathbf{D}}_{II}^{-1}, \qquad \mathbf{D}_{RL} = \tilde{\mathbf{D}}_{RL} - \tilde{\mathbf{D}}_{RI}\tilde{\mathbf{D}}_{II}^{-1}\tilde{\mathbf{D}}_{IL}, \qquad \mathbf{D}_{RR} = \tilde{\mathbf{D}}_{RR} - \tilde{\mathbf{D}}_{RI}\tilde{\mathbf{D}}_{II}^{-1}\tilde{\mathbf{D}}_{IR}.$$

From Eq. (4), keeping in mind that it holds for the unit cell $(n)$, one can get a relationship between left and right quantities, as follows:

$$\begin{Bmatrix} \mathbf{q}_R^{(n)} \\ \mathbf{F}_R^{(n)} \end{Bmatrix} = \begin{bmatrix} -\mathbf{D}_{LR}^{-1}\mathbf{D}_{LL} & -\mathbf{D}_{LR}^{-1} \\ \mathbf{D}_{RL} - \mathbf{D}_{RR}\mathbf{D}_{LR}^{-1}\mathbf{D}_{LL} & -\mathbf{D}_{RR}\mathbf{D}_{LR}^{-1} \end{bmatrix} \begin{Bmatrix} \mathbf{q}_L^{(n)} \\ -\mathbf{F}_L^{(n)} \end{Bmatrix} + \begin{bmatrix} -\mathbf{D}_{LR}^{-1}\mathbf{D}_{LI} \\ \mathbf{D}_{RI} - \mathbf{D}_{RR}\mathbf{D}_{LR}^{-1}\mathbf{D}_{LI} \end{bmatrix} \mathbf{F}_I^{(n)}. \tag{5}$$

By enforcing DOFs' compatibility and load equilibrium between adjacent unit cells, i.e. $\mathbf{q}_R^{(n)} = \mathbf{q}_L^{(n+1)}$ and $\mathbf{F}_R^{(n)} = -\mathbf{F}_L^{(n+1)} + \mathbf{F}_B^{(n)}$, being $\mathbf{F}_B^{(n)}$ an external load applied to the right interface of cell $(n)$, we obtain:

$$\mathbf{u}_L^{(n+1)} = \mathbf{S}\mathbf{u}_L^{(n)} + \mathbf{b}^{(n)}, \tag{6}$$

with:

$$\mathbf{u}_L^{(n)} = \begin{Bmatrix} \mathbf{q}_L^{(n)} \\ -\mathbf{F}_L^{(n)} \end{Bmatrix}, \qquad \mathbf{S} = \begin{bmatrix} -\mathbf{D}_{LR}^{-1}\mathbf{D}_{LL} & -\mathbf{D}_{LR}^{-1} \\ \mathbf{D}_{RL} - \mathbf{D}_{RR}\mathbf{D}_{LR}^{-1}\mathbf{D}_{LL} & -\mathbf{D}_{RR}\mathbf{D}_{LR}^{-1} \end{bmatrix}, \qquad \mathbf{b}^{(n)} = \begin{Bmatrix} \mathbf{D}_{qI}\mathbf{F}_I^{(n)} \\ \mathbf{D}_{fI}\mathbf{F}_I^{(n)} - \mathbf{F}_B^{(n)} \end{Bmatrix},$$

being $\mathbf{D}_{qI} = -\mathbf{D}_{LR}^{-1}\mathbf{D}_{LI}$ and $\mathbf{D}_{fI} = \mathbf{D}_{RI} - \mathbf{D}_{RR}\mathbf{D}_{LR}^{-1}\mathbf{D}_{LI}$. Based on the recurrence embedded in Eq. (6), it is possible to arrive at relationships between $\mathbf{u}_L^{(n+1)}$ and $\mathbf{u}_L^{(1)}$, as well as between $\mathbf{u}_L^{(N+1)}$ and $\mathbf{u}_L^{(n)}$:

$$\mathbf{u}_L^{(n+1)} = \mathbf{S}^n\mathbf{u}_L^{(1)} + \sum_{k=1}^{n}\mathbf{S}^{n-k}\mathbf{b}^{(k)}, \qquad \mathbf{u}_L^{(N+1)} = \mathbf{S}^{N+1-n}\mathbf{u}_L^{(n)} + \sum_{k=n}^{N}\mathbf{S}^{N-k}\mathbf{b}^{(k)}. \tag{7}$$

### 2.2.2. Determination of Wave Modes

By invoking periodic boundary conditions (BCs) through the Bloch-Floquet theorem, in other words $\mathbf{u}_L^{(n+1)} = e^{-\mathrm{i}k_j\Delta}\mathbf{u}_L^{(n)} = \mu_j\mathbf{u}_L^{(n)}$, being $\Delta$ the length of the unit cell along the propagation direction and $\mu_j$ the propagation constant, and by assuming no external loads, from Eq. (6) we can obtain a standard eigenvalue problem, $\left(\mathbf{S} - \mu_j\mathbf{I}\right)\boldsymbol{\phi}_j = \mathbf{0}$. Its solution are the eigenpairs $\mu_j$ and $\boldsymbol{\phi}_j$ $(j = 1, ..., 2n_b)$, being $n_b$ the number of DOFs pertaining to the left interface of the unit cell. Wavenumbers can be obtained using $k_j = (\ln\mu_j)/(-\mathrm{i}\Delta)$. Purely real and purely imaginary wavenumbers are related to propagating and evanescent waves, respectively, whereas a complex wavenumber characterizes an oscillating decaying wave.

The solution of the previously mentioned eigenproblem is not straightforward, nevertheless, because $\boldsymbol{\phi}_j$ comprises both displacements and loads, whose values can be largely disparate (Waki *et al.*, 2009b; Mencik, 2014). As an alternative, we can consider (Zhong and Williams, 1995; Mencik and Duhamel, 2015):

$$\left[\left(\mathbf{N}\mathbf{J}\mathbf{L}^{\mathrm{T}} + \mathbf{L}\mathbf{J}\mathbf{N}^{\mathrm{T}}\right) - \lambda_j\mathbf{L}\mathbf{J}\mathbf{L}^{\mathrm{T}}\right]\mathbf{z}_j = \mathbf{0}, \tag{8}$$

being:

$$\mathbf{L} = \begin{bmatrix} \mathbf{0} & \mathbf{I} \\ \mathbf{D}_{LR} & \mathbf{0} \end{bmatrix}, \qquad \mathbf{N} = \begin{bmatrix} \mathbf{D}_{RL} & \mathbf{0} \\ -\left(\mathbf{D}_{LL} + \mathbf{D}_{RR}\right) & -\mathbf{I} \end{bmatrix}, \qquad \mathbf{J} = \begin{bmatrix} \mathbf{0} & \mathbf{I} \\ -\mathbf{I} & \mathbf{0} \end{bmatrix};$$

$\lambda_j$ and $\mathbf{z}_j$ correspond to the eigenvalues and eigenvectors of the alternative, well-conditioned eigenproblem. It can be shown that $\lambda_j = \mu_j + 1/\mu_j$, such that $\mu_j = \frac{1}{2}\left(\lambda_j \pm \sqrt{\lambda_j^2 - 4}\right)$. As for the eigenvectors of the original problem, they can be retrieved by:

$$\boldsymbol{\Phi}_j = \begin{bmatrix} \mathbf{I} & \mathbf{0} \\ \mathbf{D}_{RR} & \mathbf{I} \end{bmatrix}\mathbf{w}_j, \qquad \text{with} \quad \mathbf{w}_j = \mathbf{J}\left(\mathbf{L}^{\mathrm{T}} - \tfrac{1}{\mu_j}\mathbf{N}^{\mathrm{T}}\right)\mathbf{z}_j. \tag{9}$$

Eigenvalues and associated eigenvectors can be separated into those related to positive, $(\mu_j, \boldsymbol{\Phi}_j)$, and negative-going waves, $(\mu_j^*, \boldsymbol{\Phi}_j^*)$ $(j = 1, ..., n_b)$. If $|\mu_j| < 1$, it is related to a wave which propagates in the positive direction; otherwise, if

$|\mu_j| > 1$, the corresponding wave propagates in the negative direction. If $|\mu_j| = 1$, we can exploit the power flow of the wave mode, cf. Duhamel *et al.* (2006); Waki *et al.* (2009a).

After eigensolutions have been distinguished accordingly, they can be grouped into matrices as follows:

$$\boldsymbol{\mu} = \operatorname{diag}\left(\mu_1, \ldots, \mu_{n_b}\right), \quad \boldsymbol{\Phi} = \begin{bmatrix} \boldsymbol{\phi}_1 & \ldots & \boldsymbol{\phi}_{n_b} \end{bmatrix} = \begin{bmatrix} \boldsymbol{\Phi}_q \\ \boldsymbol{\Phi}_F \end{bmatrix},$$
$$\boldsymbol{\mu}^* = \operatorname{diag}\left(\mu_1^*, \ldots, \mu_{n_b}^*\right), \quad \boldsymbol{\Phi}^* = \begin{bmatrix} \boldsymbol{\phi}_1^* & \ldots & \boldsymbol{\phi}_{n_b}^* \end{bmatrix} = \begin{bmatrix} \boldsymbol{\Phi}_q^* \\ \boldsymbol{\Phi}_F^* \end{bmatrix}, \quad (10)$$

where subscripts $q$ and $F$ identify partitions of the eigenvectors which are related to DOFs and loads.

### 2.2.3. Forced Response Computation

Using the wave modes, we can write the state vector and external loads on the unit cell $(n)$ as $\mathbf{u}_L^{(n)} = \boldsymbol{\Phi}\mathbf{Q}^{(n)} + \boldsymbol{\Phi}^*\mathbf{Q}^{*(n)}$ and $\mathbf{b}^{(n)} = \boldsymbol{\Phi}\mathbf{Q}_B^{(n)} + \boldsymbol{\Phi}^*\mathbf{Q}_B^{*(n)}$, where $\mathbf{Q}^{(n)}$, $\mathbf{Q}^{*(n)}$, $\mathbf{Q}_B^{(n)}$ and $\mathbf{Q}_B^{*(n)}$ are amplitude vectors. After some manipulations of Eq. (7), and admitting eigenvectors have been orthonormalized such that $\boldsymbol{\Phi}^{*\mathrm{T}}\mathbf{J}\boldsymbol{\Phi} = -\boldsymbol{\Phi}^{\mathrm{T}}\mathbf{J}\boldsymbol{\Phi}^* = \mathbf{I}$ and $\boldsymbol{\Phi}^{\mathrm{T}}\mathbf{J}\boldsymbol{\Phi} = \boldsymbol{\Phi}^{*\mathrm{T}}\mathbf{J}\boldsymbol{\Phi}^* = \mathbf{0}$, we get:

$$\mathbf{Q}^{(n)} = \boldsymbol{\mu}^{n-1}\mathbf{Q}^{(1)} + \sum_{k=1}^{n-1} \boldsymbol{\mu}^{n-k-1}\mathbf{Q}_B^{(k)}, \qquad \mathbf{Q}^{*(n)} = \boldsymbol{\mu}^{N+1-n}\mathbf{Q}^{*(N+1)} - \sum_{k=n}^{N} \boldsymbol{\mu}^{k-n+1}\mathbf{Q}_B^{*(k)}, \quad (11)$$

being:

$$\mathbf{Q}_B^{(k)} = \left(\boldsymbol{\mu}\boldsymbol{\Phi}_q^{*\mathrm{T}}\mathbf{D}_{LI} + \boldsymbol{\Phi}_q^{*\mathrm{T}}\mathbf{D}_{RI}\right)\mathbf{F}_I^{(k)} - \boldsymbol{\Phi}_q^{*\mathrm{T}}\mathbf{F}_B^{(k)}, \qquad \mathbf{Q}_B^{*(k)} = -\left(\boldsymbol{\mu}^*\boldsymbol{\Phi}_q^{\mathrm{T}}\mathbf{D}_{LI} + \boldsymbol{\Phi}_q^{\mathrm{T}}\mathbf{D}_{RI}\right)\mathbf{F}_I^{(k)} + \boldsymbol{\Phi}_q^{\mathrm{T}}\mathbf{F}_B^{(k)}. \quad (12)$$

Recalling that the state vector contains information related to DOFs and loads, as well as the partition introduced in Eq. (10), we can obtain, for instance:

$$\mathbf{q}_L^{(n)} = \boldsymbol{\Phi}_q\boldsymbol{\mu}^{n-1}\mathbf{Q} + \boldsymbol{\Phi}_q^*\boldsymbol{\mu}^{N+1-n}\mathbf{Q}^* + \boldsymbol{\Phi}_q \sum_{k=1}^{n-1} \boldsymbol{\mu}^{n-k-1}\mathbf{Q_B}^{(k)} - \boldsymbol{\Phi}_q^* \sum_{k=n}^{N} \boldsymbol{\mu}^{k+1-n}\mathbf{Q_B}^{*(k)}, \quad (13)$$

$$-\mathbf{F}_L^{(n)} = \boldsymbol{\Phi}_F\boldsymbol{\mu}^{n-1}\mathbf{Q} + \boldsymbol{\Phi}_F^*\boldsymbol{\mu}^{N+1-n}\mathbf{Q}^* + \boldsymbol{\Phi}_F \sum_{k=1}^{n-1} \boldsymbol{\mu}^{n-k-1}\mathbf{Q_B}^{(k)} - \boldsymbol{\Phi}_F^* \sum_{k=n}^{N} \boldsymbol{\mu}^{k+1-n}\mathbf{Q_B}^{*(k)}, \quad (14)$$

with $\mathbf{Q} \equiv \mathbf{Q}^{(1)}$ and $\mathbf{Q}^* \equiv \mathbf{Q}^{*(N+1)}$. These last equations can be used in conjunction with BCs, to establish a frequency-dependent linear system of equations, which enables the calculation of $\mathbf{Q}$ and $\mathbf{Q}^*$. After knowing these quantities, other relevant results can be evaluated as required.

## 2.3. Consideration of Coupling Between Structures Modeled by SEM and WFEM

A connection between a HS and a MS can be modeled by a linear spring, with stiffness $k$, so the force that each of these experiences can be expressed by $F = \pm k(q_h - q_m)$, where $q_h$ and $q_m$ represent the DOFs of the HS and MS, respectively, which are involved in the coupling. This reasoning can be generalized to take into account multiple couplings. The DOFs of the HS which participate in a particular connection can be obtained from $\mathbf{B}_h\bar{\mathbf{p}}^{(g)}$, where $\mathbf{B}_h$ is a Boolean matrix. (A bar is added over symbols to highlight that the quantity is related to the case of coupled dynamics between the HS and MS.) As to the DOFs of the MS, they can be similarly retrieved using $\mathbf{B}_m\bar{\tilde{\mathbf{q}}} = \mathbf{B}_m\boldsymbol{\alpha}\bar{\mathbf{q}}$.

Based on these, the force due to a connection which acts on $\mathbf{B}_h\bar{\mathbf{p}}^{(g)}$ can be expressed as $\mathbf{F}_h = \mathbf{B}_h^{\mathrm{T}}\mathbf{k}\mathbf{B}_m\boldsymbol{\alpha}\bar{\mathbf{q}} - \mathbf{B}_h^{\mathrm{T}}\mathbf{k}\mathbf{B}_h\bar{\mathbf{p}}^{(g)}$. The force which acts on $\mathbf{B}_m\bar{\tilde{\mathbf{q}}}$, after being projected using the CB transformation matrix, results equal to $\mathbf{F}_m = \boldsymbol{\alpha}^{\mathrm{T}}\mathbf{B}_m^{\mathrm{T}}\mathbf{k}\mathbf{B}_h\bar{\mathbf{p}}^{(g)} - \boldsymbol{\alpha}^{\mathrm{T}}\mathbf{B}_m^{\mathrm{T}}\mathbf{k}\mathbf{B}_m\boldsymbol{\alpha}\bar{\mathbf{q}}$. In the previous, $\mathbf{k}$ is a translational-spring stiffness matrix, of size $2\times 2$, with components $k_x$, $k_y$, $k_{xy}$ and $k_{yx}$.

Concerning the modifications needed for the WFEM, for a unit cell which is coupled to the HS, Eq. (4) needs to be changed to:

$$\begin{bmatrix} \tilde{\mathbf{D}}_{LL} & \tilde{\mathbf{D}}_{LR} & \tilde{\mathbf{D}}_{LI} \\ \tilde{\mathbf{D}}_{RL} & \tilde{\mathbf{D}}_{RR} & \tilde{\mathbf{D}}_{RI} \\ \tilde{\mathbf{D}}_{IL} & \tilde{\mathbf{D}}_{IR} & \tilde{\mathbf{D}}_{II} \end{bmatrix} \begin{Bmatrix} \bar{\mathbf{q}}_L \\ \bar{\mathbf{q}}_R \\ \bar{\mathbf{q}}_I \end{Bmatrix} = \begin{Bmatrix} \bar{\mathbf{F}}_L \\ \bar{\mathbf{F}}_R \\ \bar{\mathbf{F}}_I \end{Bmatrix} + \begin{Bmatrix} (\mathbf{F}_m)_L \\ (\mathbf{F}_m)_R \\ (\mathbf{F}_m)_I \end{Bmatrix} \quad \Rightarrow$$
$$\Rightarrow \quad \begin{bmatrix} \bar{\mathbf{D}}_{LI}\bar{\mathbf{F}}_I \\ \bar{\mathbf{D}}_{RI}\bar{\mathbf{F}}_I \end{bmatrix} + \begin{bmatrix} \bar{\mathbf{D}}_{LL} & \bar{\mathbf{D}}_{LR} \\ \bar{\mathbf{D}}_{RL} & \bar{\mathbf{D}}_{RR} \end{bmatrix} \begin{Bmatrix} \bar{\mathbf{q}}_L \\ \bar{\mathbf{q}}_R \end{Bmatrix} + \begin{bmatrix} (\bar{\mathbf{D}}_{LI}\mathbf{i} - \mathbf{l})\bar{\mathbf{p}}^{(g)} \\ (\bar{\mathbf{D}}_{RI}\mathbf{i} - \mathbf{r})\bar{\mathbf{p}}^{(g)} \end{bmatrix} = \begin{Bmatrix} \bar{\mathbf{F}}_L \\ \bar{\mathbf{F}}_R \end{Bmatrix}, \quad (15)$$

where:

$$\bar{\mathbf{D}}_{LI} = \tilde{\bar{\mathbf{D}}}_{LI}\tilde{\bar{\mathbf{D}}}_{II}^{-1}, \quad \bar{\mathbf{D}}_{LL} = \tilde{\bar{\mathbf{D}}}_{LL} - \tilde{\bar{\mathbf{D}}}_{LI}\tilde{\bar{\mathbf{D}}}_{II}^{-1}\tilde{\bar{\mathbf{D}}}_{IL}, \quad \bar{\mathbf{D}}_{LR} = \tilde{\bar{\mathbf{D}}}_{LR} - \tilde{\bar{\mathbf{D}}}_{LI}\tilde{\bar{\mathbf{D}}}_{II}^{-1}\tilde{\bar{\mathbf{D}}}_{IR},$$
$$\bar{\mathbf{D}}_{RI} = \tilde{\bar{\mathbf{D}}}_{RI}\tilde{\bar{\mathbf{D}}}_{II}^{-1}, \quad \bar{\mathbf{D}}_{RL} = \tilde{\bar{\mathbf{D}}}_{RL} - \tilde{\bar{\mathbf{D}}}_{RI}\tilde{\bar{\mathbf{D}}}_{II}^{-1}\tilde{\bar{\mathbf{D}}}_{IL}, \quad \bar{\mathbf{D}}_{RR} = \tilde{\bar{\mathbf{D}}}_{RR} - \tilde{\bar{\mathbf{D}}}_{RI}\tilde{\bar{\mathbf{D}}}_{II}^{-1}\tilde{\bar{\mathbf{D}}}_{IR},$$
$$\mathbf{i} = \boldsymbol{\alpha}_I^{\mathrm{T}}\mathbf{B}_m^{\mathrm{T}}\mathbf{k}\mathbf{B}_h, \qquad \mathbf{l} = \boldsymbol{\alpha}_L^{\mathrm{T}}\mathbf{B}_m^{\mathrm{T}}\mathbf{k}\mathbf{B}_h, \qquad \mathbf{r} = \boldsymbol{\alpha}_R^{\mathrm{T}}\mathbf{B}_m^{\mathrm{T}}\mathbf{k}\mathbf{B}_h.$$

One can then manipulate Eq. (15) to show that:

$$\begin{Bmatrix} \bar{\mathbf{q}}_R^{(n)} \\ \bar{\mathbf{F}}_R^{(n)} \end{Bmatrix} = \begin{bmatrix} -\bar{\mathbf{D}}_{LR}^{-1}\bar{\mathbf{D}}_{LL} & -\bar{\mathbf{D}}_{LR}^{-1} \\ \bar{\mathbf{D}}_{RL} - \bar{\mathbf{D}}_{RR}\bar{\mathbf{D}}_{LR}^{-1}\bar{\mathbf{D}}_{LL} & -\bar{\mathbf{D}}_{RR}\bar{\mathbf{D}}_{LR}^{-1} \end{bmatrix} \begin{Bmatrix} \bar{\mathbf{q}}_L^{(n)} \\ -\bar{\mathbf{F}}_L^{(n)} \end{Bmatrix} + \begin{bmatrix} -\bar{\mathbf{D}}_{LR}^{-1}\bar{\mathbf{D}}_{LI} \\ \bar{\mathbf{D}}_{RI} - \bar{\mathbf{D}}_{RR}\bar{\mathbf{D}}_{LR}^{-1}\bar{\mathbf{D}}_{LI} \end{bmatrix} \bar{\mathbf{F}}_I^{(n)} + \begin{bmatrix} -\bar{\mathbf{D}}_{LR}^{-1}(\bar{\mathbf{D}}_{LI}\mathbf{i} - \mathbf{l}) \\ -\bar{\mathbf{D}}_{RR}\bar{\mathbf{D}}_{LR}^{-1}(\bar{\mathbf{D}}_{LI}\mathbf{i} - \mathbf{l}) + \bar{\mathbf{D}}_{RI}\mathbf{i} - \mathbf{r} \end{bmatrix} \bar{\mathbf{p}}^{(g)}. \quad (16)$$

Conditions for DOFs' compatibility and load equilibrium between neighbor unit cells introduced before remain valid, as long as the coupling on the MS does not occur at the interface of the unit cells. Thus:

$$\bar{\mathbf{u}}_L^{(n+1)} = \bar{\mathbf{S}}\bar{\mathbf{u}}_L^{(n)} + \bar{\mathbf{b}}^{(n)} + \mathbf{b}_c\bar{\mathbf{p}}^{(g)}, \quad (17)$$

and $\bar{\mathbf{u}}_L^{(n)}$, $\bar{\mathbf{S}}$ and $\bar{\mathbf{b}}^{(n)}$ being analogous to $\mathbf{u}_L^{(n)}$, $\mathbf{S}$ and $\mathbf{b}^{(n)}$ [cf. Eq. (6)], whereas:

$$\mathbf{b}_c = \begin{bmatrix} -\bar{\mathbf{D}}_{LR}^{-1}(\bar{\mathbf{D}}_{LI}\mathbf{i} - \mathbf{l}) \\ -\bar{\mathbf{D}}_{RR}\bar{\mathbf{D}}_{LR}^{-1}(\bar{\mathbf{D}}_{LI}\mathbf{i} - \mathbf{l}) + \bar{\mathbf{D}}_{RI}\mathbf{i} - \mathbf{r} \end{bmatrix}. \quad (18)$$

Equation (7) and those described in Sec. 2.2.2 remain valid, provided the inclusion of the bar superscript over the terms related to the coupled problem dynamics. Using the wave mode expansion, we can obtain:

$$\bar{\mathbf{Q}}^{(n)} = \bar{\mu}^{n-1}\bar{\mathbf{Q}}^{(1)} + \sum_{k=1}^{n-1}\bar{\mu}^{n-k-1}\tilde{\bar{\mathbf{Q}}}_B^{(k)}, \qquad \bar{\mathbf{Q}}^{*(n)} = \bar{\mu}^{N+1-n}\bar{\mathbf{Q}}^{*(N+1)} - \sum_{k=n}^{N}\bar{\mu}^{k-n+1}\tilde{\bar{\mathbf{Q}}}_B^{*(k)}, \quad (19)$$

being $\tilde{\bar{\mathbf{Q}}}_B^{(k)} = \bar{\mathbf{Q}}_B^{(k)} + \bar{\mathbf{Q}}_C\bar{\mathbf{p}}^{(g)}$ and $\tilde{\bar{\mathbf{Q}}}_B^{*(k)} = \bar{\mathbf{Q}}_B^{*(k)} + \bar{\mathbf{Q}}_C^{*}\bar{\mathbf{p}}^{(g)}$, with $\bar{\mathbf{Q}}_B^{(k)}$ and $\bar{\mathbf{Q}}_B^{*(k)}$ analogous to $\mathbf{Q}_B^{(k)}$ and $\mathbf{Q}_B^{*(k)}$. Furthermore:

$$\bar{\mathbf{Q}}_C = \left(\bar{\mu}\bar{\mathbf{\Phi}}_q^{*\mathrm{T}}\bar{\mathbf{D}}_{LI} + \bar{\mathbf{\Phi}}_q^{*\mathrm{T}}\bar{\mathbf{D}}_{RI}\right)\mathbf{i} - \bar{\mu}\bar{\mathbf{\Phi}}_q^{*\mathrm{T}}\mathbf{l} - \bar{\mathbf{\Phi}}_q^{*\mathrm{T}}\mathbf{r}, \qquad \bar{\mathbf{Q}}_C^{*} = -\left(\bar{\mu}^{*}\bar{\mathbf{\Phi}}_q^{\mathrm{T}}\bar{\mathbf{D}}_{LI} + \bar{\mathbf{\Phi}}_q^{\mathrm{T}}\bar{\mathbf{D}}_{RI}\right)\mathbf{i} + \bar{\mu}^{*}\bar{\mathbf{\Phi}}_q^{\mathrm{T}}\mathbf{l} + \bar{\mathbf{\Phi}}_q^{\mathrm{T}}\mathbf{r}.$$

After some developments, it is possible to obtain results which are similar to Eqs. (13) and (14):

$$\begin{aligned}\bar{\mathbf{q}}_L^{(n)} = {} & \bar{\mathbf{\Phi}}_q\bar{\mu}^{n-1}\bar{\mathbf{Q}} + \bar{\mathbf{\Phi}}_q^{*}\bar{\mu}^{N+1-n}\bar{\mathbf{Q}}^{*} + \bar{\mathbf{\Phi}}_q\sum_{k=1}^{n-1}\bar{\mu}^{n-k-1}\bar{\mathbf{Q}}_B^{(k)} - \bar{\mathbf{\Phi}}_q^{*}\sum_{k=n}^{N}\bar{\mu}^{k+1-n}\bar{\mathbf{Q}}_B^{*(k)} \\ & + \left(\bar{\mathbf{\Phi}}_q\sum_{k=1}^{n-1}\bar{\mu}^{n-k-1}\bar{\mathbf{Q}}_C - \bar{\mathbf{\Phi}}_q^{*}\sum_{k=n}^{N}\bar{\mu}^{k+1-n}\bar{\mathbf{Q}}_C^{*}\right)\bar{\mathbf{p}}^{(g)}, \quad (20)\\ -\bar{\mathbf{F}}_L^{(n)} = {} & \bar{\mathbf{\Phi}}_F\bar{\mu}^{n-1}\bar{\mathbf{Q}} + \bar{\mathbf{\Phi}}_F^{*}\bar{\mu}^{N+1-n}\bar{\mathbf{Q}}^{*} + \bar{\mathbf{\Phi}}_F\sum_{k=1}^{n-1}\bar{\mu}^{n-k-1}\bar{\mathbf{Q}}_B^{(k)} - \bar{\mathbf{\Phi}}_F^{*}\sum_{k=n}^{N}\bar{\mu}^{k+1-n}\bar{\mathbf{Q}}_B^{*(k)} \\ & + \left(\bar{\mathbf{\Phi}}_F\sum_{k=1}^{n-1}\bar{\mu}^{n-k-1}\bar{\mathbf{Q}}_C - \bar{\mathbf{\Phi}}_F^{*}\sum_{k=n}^{N}\bar{\mu}^{k+1-n}\bar{\mathbf{Q}}_C^{*}\right)\bar{\mathbf{p}}^{(g)}, \quad (21)\end{aligned}$$

where $\bar{\mathbf{Q}} \equiv \bar{\mathbf{Q}}^{(1)}$ and $\bar{\mathbf{Q}}^{*} \equiv \bar{\mathbf{Q}}^{*(N+1)}$. The previous equations can then be used in conjunction with BCs applied to the MS, to establish equations relating $\bar{\mathbf{Q}}$, $\bar{\mathbf{Q}}^{*}$, and $\bar{\mathbf{p}}^{(g)}$.

To determine these unknowns, one also needs to consider the HS dynamics. The SEM equations used to model it need to be modified to take into account the coupling with the MS, i.e. we must have $\mathbf{H}^{(g)}\bar{\mathbf{p}}^{(g)} = \mathbf{f}^{(g)} + \mathbf{F}_h$, with $\mathbf{F}_h$ defined previously. After various manipulation, it is possible to arrive at:

$$\left(\mathbf{H}^{(g)} + \mathbf{B}_h^{\mathrm{T}}\mathbf{k}\mathbf{B}_h - \mathbf{B}_h^{\mathrm{T}}\mathbf{k}\mathbf{B}_m\boldsymbol{\alpha}\boldsymbol{\epsilon}\right)\bar{\mathbf{p}}^{(g)} - \mathbf{B}_h^{\mathrm{T}}\mathbf{k}\mathbf{B}_m\boldsymbol{\alpha}\boldsymbol{\beta}\begin{Bmatrix}\bar{\mathbf{Q}} \\ \bar{\mathbf{Q}}^{*}\end{Bmatrix} = \mathbf{f}^{(g)} + \mathbf{B}_h^{\mathrm{T}}\mathbf{k}\mathbf{B}_m\boldsymbol{\alpha}\boldsymbol{\psi}, \quad (22)$$

where:

$$\boldsymbol{\epsilon} = \begin{bmatrix} -\bar{\mathbf{\Phi}}_q^{*}\bar{\mu}\bar{\mathbf{Q}}_C^{*} \\ \bar{\mathbf{\Phi}}_q\bar{\mathbf{Q}}_C \\ \tilde{\bar{\mathbf{D}}}_{II}^{-1}\left(\tilde{\bar{\mathbf{D}}}_{IL}\bar{\mathbf{\Phi}}_q^{*}\bar{\mu}\bar{\mathbf{Q}}_C^{*} - \tilde{\bar{\mathbf{D}}}_{IR}\bar{\mathbf{\Phi}}_q\bar{\mathbf{Q}}_C + \mathbf{i}\right) \end{bmatrix}, \qquad \boldsymbol{\psi} = \begin{Bmatrix} -\bar{\mathbf{\Phi}}_q^{*}\bar{\mu}\bar{\mathbf{Q}}_B^{*(1)} \\ \bar{\mathbf{\Phi}}_q\bar{\mathbf{Q}}_B^{(1)} \\ \tilde{\bar{\mathbf{D}}}_{II}^{-1}\left(\tilde{\bar{\mathbf{D}}}_{IL}\bar{\mathbf{\Phi}}_q^{*}\bar{\mu}\bar{\mathbf{Q}}_B^{*(1)} - \tilde{\bar{\mathbf{D}}}_{IR}\bar{\mathbf{\Phi}}_q\bar{\mathbf{Q}}_B^{(1)} + \bar{\mathbf{F}}_I^{(1)}\right) \end{Bmatrix},$$

$$\boldsymbol{\beta} = \begin{bmatrix} \bar{\mathbf{\Phi}}_q & \bar{\mathbf{\Phi}}_q^{*}\bar{\mu} \\ \bar{\mathbf{\Phi}}_q\bar{\mu} & \bar{\mathbf{\Phi}}_q^{*} \\ -\tilde{\bar{\mathbf{D}}}_{II}^{-1}\left(\tilde{\bar{\mathbf{D}}}_{IL}\bar{\mathbf{\Phi}}_q + \tilde{\bar{\mathbf{D}}}_{IR}\bar{\mathbf{\Phi}}_q\bar{\mu}\right) & -\tilde{\bar{\mathbf{D}}}_{II}^{-1}\left(\tilde{\bar{\mathbf{D}}}_{IL}\bar{\mathbf{\Phi}}_q^{*}\bar{\mu} + \tilde{\bar{\mathbf{D}}}_{IR}\bar{\mathbf{\Phi}}_q^{*}\right) \end{bmatrix}.$$

The complete problem which needs to be solved for the coupled system (for each frequency) then comprises equations established using Eqs. (20) and (21), as well as (22). Coupling-related terms can be clearly identified when comparing these with corresponding ones presented in Sec. 2.1 and 2.2.

## 3. NUMERICAL SIMULATIONS

The main aim of the numerical simulations considered here is to validate the procedure presented earlier for analyzing the dynamic behavior of coupled structures modeled by the SEM and WFEM. For this purpose, one considers the system depicted in Fig. 1. The material of the HS and MS are assumed to be the same, and to have linear elastic behavior, with $E = 30$ GPa, $\nu = 0.3$ and $\rho = 2200$ kg/m$^3$. Damping is not taken into account. The HS is a straight beam with length of 1.3 m, width of 25.4 mm, and thickness of 4.76 mm. The unit cell mesh considered for the MS is shown in Fig. 3, comprising 49 nodes. Both the base and height of the unit cell measure 100 mm. The finite element modeling has been performed with the Altair® HyperMesh® 2021 software, using the four node CQUAD4 element, with two translational DOFs per node. Plane stress state was assumed, with thickness input (taken as 10 mm). The total number of unit cells which compose the MS was taken as $N = 10$. Within the proposed approach for taking into account the coupling between the MS and the HS, one assumes that unit cells which get coupled correspond to individual waveguides. For this reason, in our example, the MS is treated as being composed of three distinct waveguides, with $N_1 = N_3 = 1$ and $N_2 = 8$.

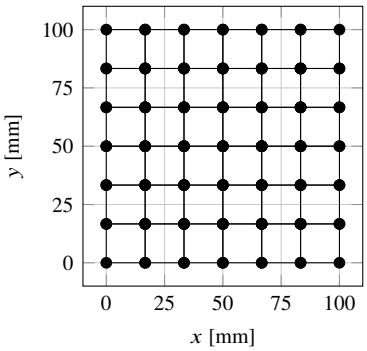


Figure 3: **Geometry and finite element mesh for the unit cell of the MS.**

One should highlight that the considered unit cell does not provide any special or unusual behavior for the periodic structure dynamics which is attached to the HS: the one-dimensional periodic structure should behave as a straight beam. This has been considered to simplify analysis, since at the current state of our research, the aim was to validate the modeling approach and in-house implemented codes. Despite the rather simple unit cell, in the following we still adopt the MS description for the not-so-special one-dimensional periodic structure.

With regards to the coupling between HS and MS, it takes place at two locations, cf. Fig. 1. The nodes of the MS which participate in the couplings are localized immediately adjacent to the boundaries of the relevant unit cells, as suggested in the same figure. Also, these nodes are in the middle of the height of the unit cell.

Assuming that the coupling occurs independently in the $x$ and $y$-directions, i.e. $k_{xy} = k_{yx} = 0$, we are able to obtain the dispersion curves for the uncoupled and coupled unit cells of the MS. For assessing the coupled unit cell dispersion relation, it is assumed that the HS has no motion (fixed interface condition). Two values were considered for the coupling stiffness, namely 1 MN/m ("soft" spring) and 1 GN/m ("hard" spring).

Figure 4a shows in solid blue lines (——) the well known wave modes found for a typical beam structure, obtained from the eigenproblem mentioned in Sec. 2.2.2: a longitudinal propagating wave mode and two bending wave modes (one propagating and the other evanescent) (Doyle, 2020). Although not shown, these curves are in perfect agreement with analytical results, presented in Sec. 2.1, i.e. $k_j$ ($j = 1, ..., 6$). The presence of longitudinal soft and hard springs (while taking $k_y = 0$) changes somewhat the unit cell dynamics, as can be observed by red dash-dotted line (-·-·-) and magenta dashed line (- - -), respectively. For the soft spring, we can see the occurrence of a cut-on frequency around 330 Hz for the longitudinal wave mode. As the coupling spring stiffness increases, the cut-on frequency gets larger, such that, for the hard coupling spring, the longitudinal wave mode becomes evanescent in the whole analyzed frequency range. The appearance of a cut-on frequency on the dispersion curve for the longitudinal mode bears relation to the dynamics of a rod which rests on an elastic foundation (Doyle, 2020).

Figure 4b shows similar results, but related to the case in which coupling exists along the $y$ direction, only (i.e. $k_x = 0$). Similarly to the previous case, the attachment of a soft or hard coupling-spring in a bending-related DOF leads to changes in the unit cell dynamics, as can be observed by red dash-dotted (-·-·-) and magenta dashed (- - -) curves. For the soft spring, we can see the occurrence of a cut-on frequency around 340 Hz for one of the bending modes. In other words, the propagating bending wave mode found in the uncoupled unit cell becomes evanescent up to 340 Hz. The other bending wave mode is evanescent over the entire analyzed frequency range, although its real part suggests its propagation up to 340 Hz.

It is noteworthy that, in both coupling situations, the longitudinal and bending dynamics of the MS appear to be independent, i.e. the longitudinal coupling does not affect the bending dispersion curves and vice-versa. We imagine these results because the coupling nodes on the MS are located in the middle of the unit cells' height, so along the neutral fiber of the beam. If that was not the case, longitudinal and bending behavior could be simultaneously affected by a single coupling spring, placed either along $x$ or $y$.

To better clarify how the forced response of the coupled system can be obtained, further developments are now presented

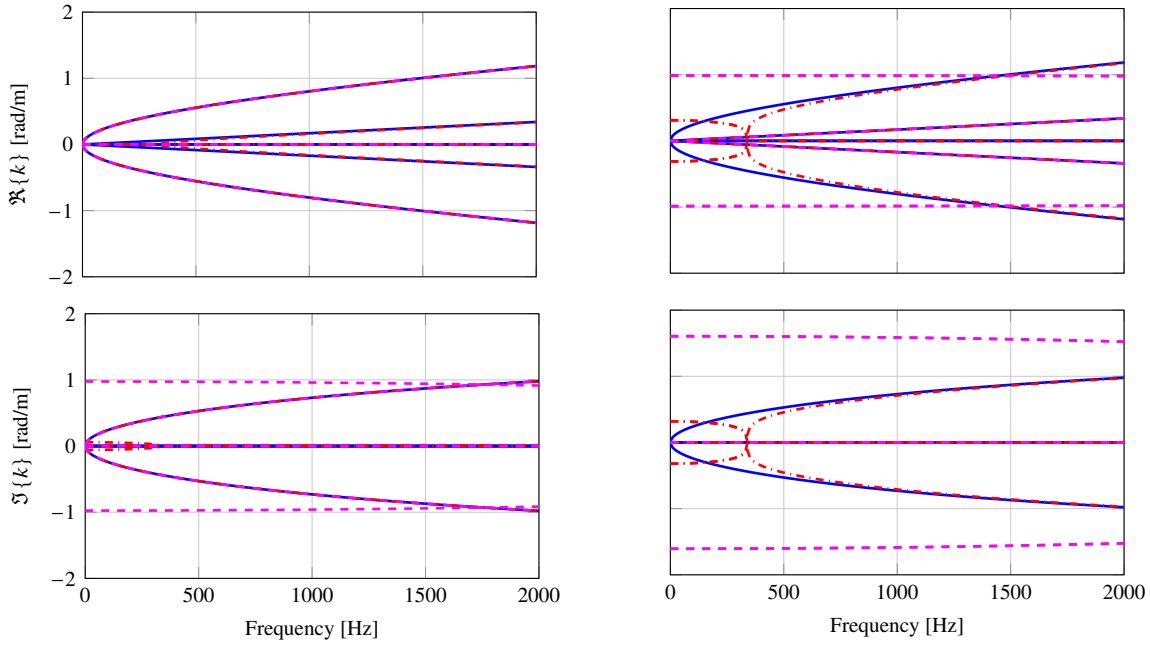


(a) Longitudinal coupling ($k_y = k_{xy} = k_{yx} = 0$)

(b) Transversal coupling ($k_x = k_{xy} = k_{yx} = 0$)

Figure 4: **Dispersion curves for the uncoupled (——) and coupled unit cells (-·-·-: 1 MN/m; - - -: 1 GN/m).**

for the considered problem. As a matter of fact, BCs need to be taken into account. For the HS, since it is clamped-free, the DOFs located at its left extremity must be blocked. (This can be done by deleting appropriate columns of $\bar{\mathbf{H}}^{(g)}$ and neglecting the rows/equations associated with the same DOFs, similarly to what is done in the traditional FEM.) For the MS, free-free BCs need to be imposed, i.e. $\bar{\mathbf{F}}_L^{(1)}\big|_1 = \mathbf{0}$ and $\bar{\mathbf{F}}_R^{(1)}\big|_3 = \mathbf{0}$. (The notation $|_j$ is used to denote that a given quantity is related to waveguide $j$ of the MS, $j = 1, 2, 3$.) So, invoking Eq. (21), it is possible to obtain:

$$\left(\bar{\mathbf{\Phi}}_F\bar{\mathbf{Q}} + \bar{\mathbf{\Phi}}_F^*\bar{\mu}\bar{\mathbf{Q}}^* - \bar{\mathbf{\Phi}}_F^*\bar{\mu}\bar{\mathbf{Q}}_C^*\bar{\mathbf{p}}^{(g)}\right)\Big|_1 = \mathbf{0}, \tag{23}$$

$$\left(\bar{\mathbf{\Phi}}_F\bar{\mu}\bar{\mathbf{Q}} + \bar{\mathbf{\Phi}}_F^*\bar{\mathbf{Q}}^* + \bar{\mathbf{\Phi}}_F\bar{\mathbf{Q}}_C\bar{\mathbf{p}}^{(g)}\right)\Big|_3 = \mathbf{0}. \tag{24}$$

In addition to imposing the BCs, one must guarantee the DOFs compatibility and load equilibrium between the shared boundaries of neighbor waveguides. In other words, we must have that $\bar{\mathbf{q}}_L^{(2)}\big|_1 = \bar{\mathbf{q}}_L^{(1)}\big|_2$ and $-\bar{\mathbf{F}}_L^{(2)}\big|_1 = -\bar{\mathbf{F}}_L^{(1)}\big|_2$; and that $\bar{\mathbf{q}}_L^{(N_2+1)}\big|_2 = \bar{\mathbf{q}}_L^{(1)}\big|_3$ and $-\bar{\mathbf{F}}_L^{(N_2+1)}\big|_2 = -\bar{\mathbf{F}}_L^{(1)}\big|_3$. From Eqs. (20) and (21), we obtain:

$$\left(\bar{\mathbf{\Phi}}_q\bar{\mu}\bar{\mathbf{Q}} + \bar{\mathbf{\Phi}}_q^*\bar{\mathbf{Q}}^* + \bar{\mathbf{\Phi}}_q\bar{\mathbf{Q}}_C\bar{\mathbf{p}}^{(g)}\right)\Big|_1 = \left(\bar{\mathbf{\Phi}}_q\bar{\mathbf{Q}} + \bar{\mathbf{\Phi}}_q^*\bar{\mu}^{N_2}\bar{\mathbf{Q}}^*\right)\Big|_2, \tag{25}$$

$$\left(\bar{\mathbf{\Phi}}_F\bar{\mu}\bar{\mathbf{Q}} + \bar{\mathbf{\Phi}}_F^*\bar{\mathbf{Q}}^* + \bar{\mathbf{\Phi}}_F\bar{\mathbf{Q}}_C\bar{\mathbf{p}}^{(g)}\right)\Big|_1 = \left(\bar{\mathbf{\Phi}}_F\bar{\mathbf{Q}} + \bar{\mathbf{\Phi}}_F^*\bar{\mu}^{N_2}\bar{\mathbf{Q}}^*\right)\Big|_2, \tag{26}$$

$$\left(\bar{\mathbf{\Phi}}_q\bar{\mu}^{N_2}\bar{\mathbf{Q}} + \bar{\mathbf{\Phi}}_q^*\bar{\mathbf{Q}}^*\right)\Big|_2 = \left(\bar{\mathbf{\Phi}}_q\bar{\mathbf{Q}} + \bar{\mathbf{\Phi}}_q^*\bar{\mu}\bar{\mathbf{Q}}^* - \bar{\mathbf{\Phi}}_q^*\bar{\mu}\bar{\mathbf{Q}}_C^*\bar{\mathbf{p}}^{(g)}\right)\Big|_3, \tag{27}$$

$$\left(\bar{\mathbf{\Phi}}_F\bar{\mu}^{N_2}\bar{\mathbf{Q}} + \bar{\mathbf{\Phi}}_F^*\bar{\mathbf{Q}}^*\right)\Big|_2 = \left(\bar{\mathbf{\Phi}}_F\bar{\mathbf{Q}} + \bar{\mathbf{\Phi}}_F^*\bar{\mu}\bar{\mathbf{Q}}^* - \bar{\mathbf{\Phi}}_F^*\bar{\mu}\bar{\mathbf{Q}}_C^*\bar{\mathbf{p}}^{(g)}\right)\Big|_3. \tag{28}$$

The complete system of coupled equations can be assembled by combining Eqs. (23)–(28) and Eq. (22) (after applying the BCs for the HS). It reads:

$$\begin{bmatrix} \bar{\mathbf{A}}^{(g)} & \mathbf{\eta}_1 \\ \mathbf{\eta}_2 & \bar{\mathbf{H}}^{(g)} \end{bmatrix} \begin{Bmatrix} \bar{\mathbf{Q}}^{(g)} \\ \bar{\mathbf{p}}^{(g)} \end{Bmatrix} = \begin{Bmatrix} \bar{\mathbf{F}}^{(g)} \\ \bar{\mathbf{f}}^{(g)} \end{Bmatrix}, \tag{29}$$

with $\mathbf{\eta}_1$ and $\mathbf{\eta}_2$ identified as the coupling matrices between SEM and WFEM unknowns, $\bar{\mathbf{F}}^{(g)}$ and $\bar{\mathbf{f}}^{(g)}$ vectors related to external loads and some arising terms from the coupling between HS and MS (whose expressions are not explicitly provided here, due to manuscript length constraints), $\bar{\mathbf{Q}}^{(g)} = \left\{ \bar{\mathbf{Q}}^{\mathrm{T}}\big|_1 \;\; \bar{\mathbf{Q}}^{*\mathrm{T}}\big|_1 \;\; \bar{\mathbf{Q}}^{\mathrm{T}}\big|_2 \;\; \bar{\mathbf{Q}}^{*\mathrm{T}}\big|_2 \;\; \bar{\mathbf{Q}}^{\mathrm{T}}\big|_3 \;\; \bar{\mathbf{Q}}^{*\mathrm{T}}\big|_3 \right\}^{\mathrm{T}}$ and $\bar{\mathbf{p}}^{(g)} = \left\{ U_2 \;\; V_2 \;\; \Theta_2 \;\; U_3 \;\; V_3 \;\; \Theta_3 \;\; U_4 \;\; V_4 \;\; \Theta_4 \right\}^{\mathrm{T}}$, with $U_j, V_j, \Theta_j$ the DOFs of node $j$ of the SEM mesh (cf. Fig. 1). It should be mentioned that, for the solution of Eq. 29, the WFEM-related equations are preconditioned cf. the procedure outlined by Mencik (2010). After $\bar{\mathbf{Q}}^{(g)}$ has been obtained, responses at any MS unit cell can be calculated using Eq. (13) for the uncoupled waveguide 2, or Eq. (20) for the coupled waveguides 1 and 3.

To validate the implemented codes and the developed equations, the longitudinal and bending behaviors of the system presented in Fig. 1 were investigated independently, for both soft and hard coupling springs considered previously.

Longitudinal behavior was considered when both force and responses were related to a DOF in the $x$-direction. On the other hand, the bending behavior was exploited considering that both force and responses were related to a DOF in the $y$-direction. When longitudinal behavior was analyzed, one has taken $k_y = 0$; and for analyzing bending, we have adopted $k_x = 0$.

Therefore, we defined the excitation point to be at the right side of the HS, with accelerance FRFs being obtained at the HS coupling points (nodes 2 and 3), at the driving point (node 4) and at the MS coupling points (at waveguides 1 and 3). For the WFEM, reduced wave basis were admitted for all waveguides, considering 13 wave modes which travel in the positive $x$-direction.

Concerning the longitudinal behavior, in Fig. 5 one compares results obtained using our procedure (- - -) to those computed using finite element software Altair® HyperMesh® 2021 (——). For both the soft and hard coupling spring (cf. Figs. 5a–5e and Figs. 5f–5j, respectively), it is possible to see a perfect agreement between both sets of results. To achieve this high level of precision between both results, it was necessary to employ almost all wave modes to describe the MS dynamics, and, by extension, the coupling terms ($\boldsymbol{\eta}_1$ and $\boldsymbol{\eta}_2$). This helps confirm that the inclusion of coupling springs greatly alters the behavior of the unit cell (cf. indicated by Fig. 4). One should also mention that, during tests, the use of a smaller number of wave modes could not adequately describe the dynamics of the coupled system.

Furthermore, although not shown, the use of the CB method to reduce the number of internal DOFs that describe the unit cell dynamics significantly harms the results which can be obtained by the proposed modeling approach. We suppose that the MS DOFs which participate in the coupling with the HS should not be condensed so better results can be achieved — since these DOFs are extremely important for the coupling description. Avoiding the use of the CB method does not lead to a prohibitive computational cost here, since the mesh adopted is very simple, in the sense it contains a small number of DOFs. However, the analysis of coupled structures whose MS unit cells contain many DOFs is expected to become cumbersome.

Similar results have been obtained to investigate bending behavior. Comparisons are presented in Fig. 6 for soft and hard coupling springs. Despite the high modal density found in the FRFs, responses obtained using the proposed approach agree very well with those obtained from finite element analysis.

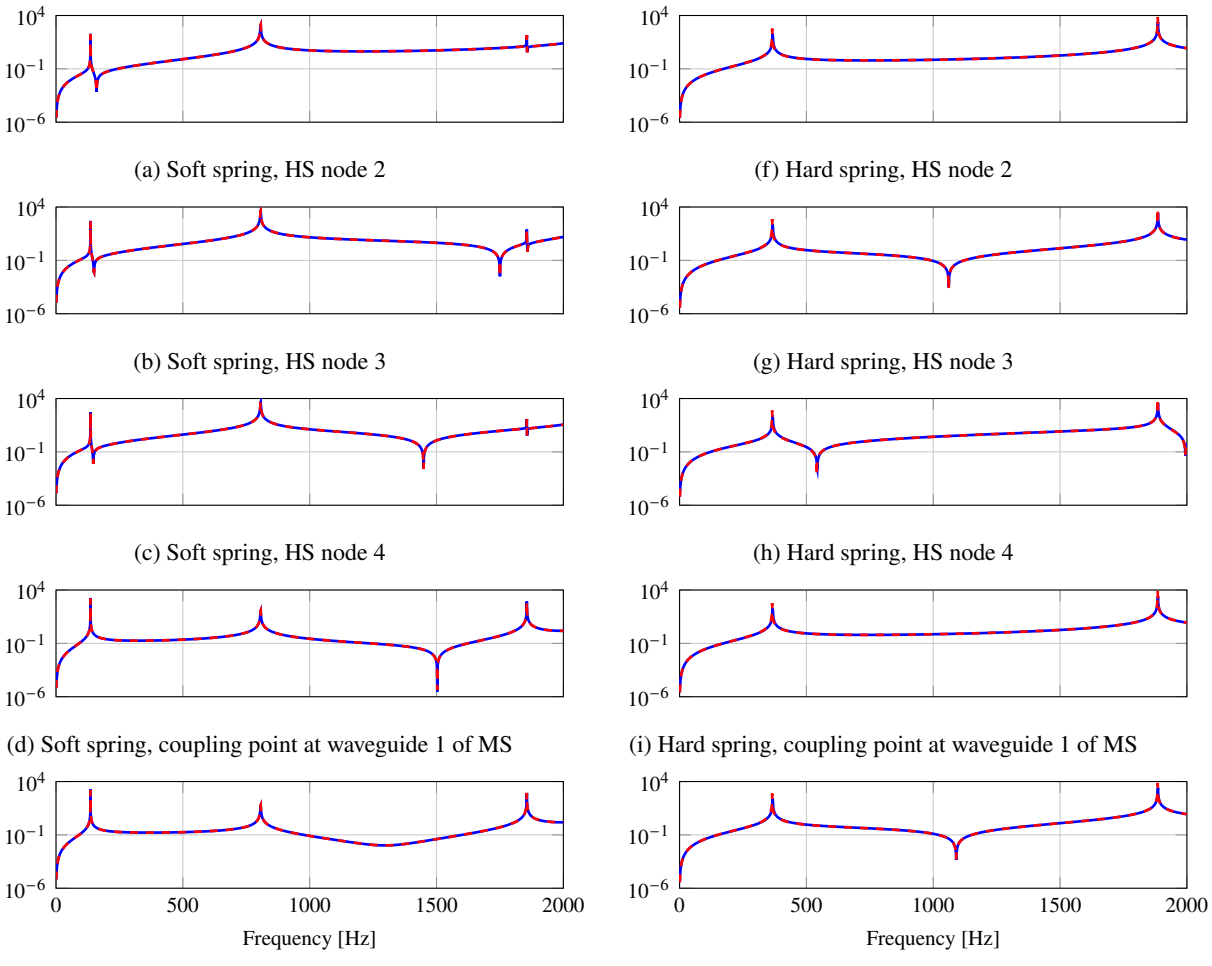


(a) Soft spring, HS node 2

(f) Hard spring, HS node 2

(b) Soft spring, HS node 3

(g) Hard spring, HS node 3

(c) Soft spring, HS node 4

(h) Hard spring, HS node 4

(d) Soft spring, coupling point at waveguide 1 of MS

(i) Hard spring, coupling point at waveguide 1 of MS

(e) Soft spring, coupling point at waveguide 3 of MS

(j) Hard spring, coupling point at waveguide 3 of MS

Figure 5: **Longitudinal accelerance FRFs [m/(s$^2$N)] obtained using the Altair® HyperMesh® 2021 finite element software (——) and our approach (- - -), considering soft and hard coupling springs.**

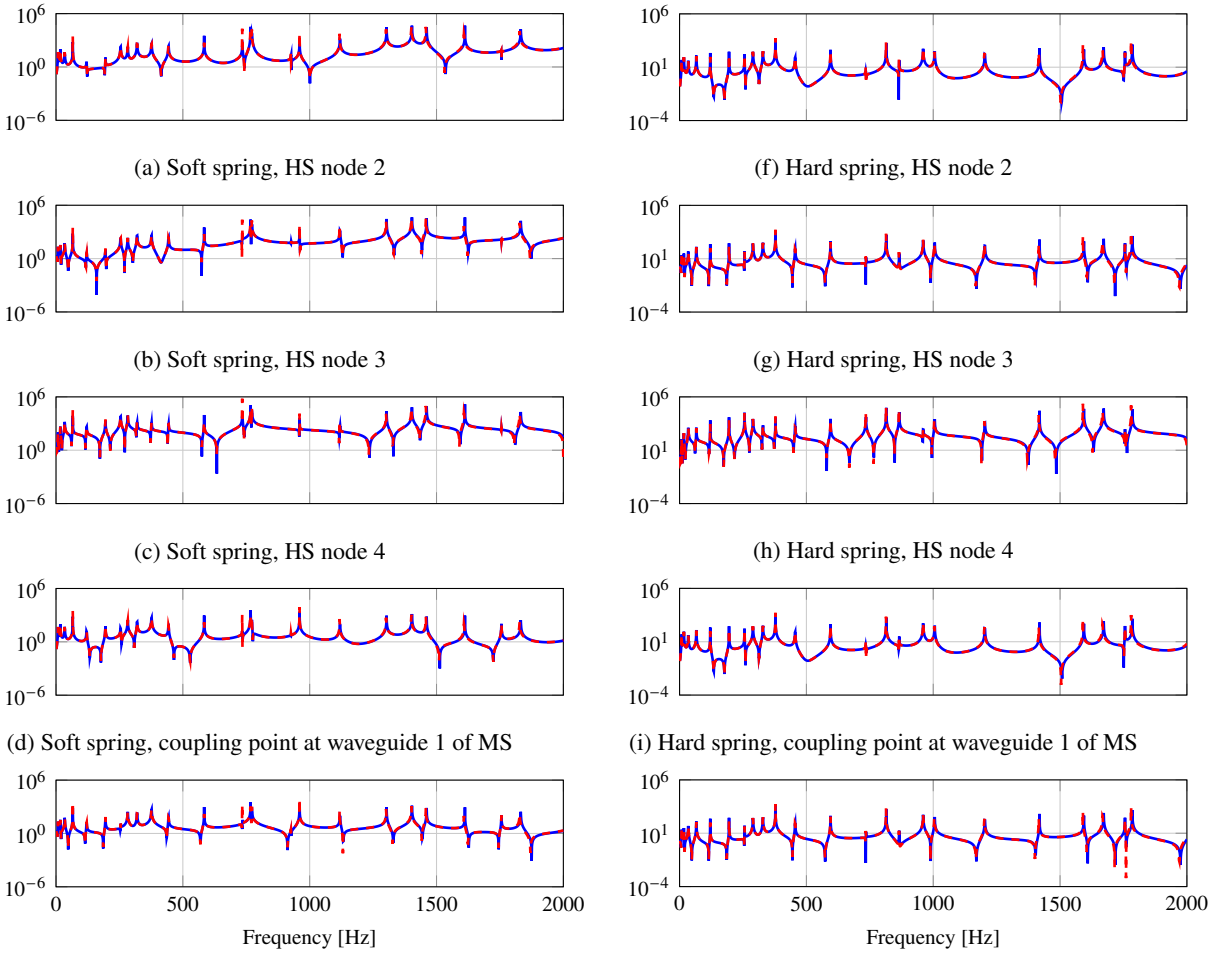


(a) Soft spring, HS node 2

(b) Soft spring, HS node 3

(c) Soft spring, HS node 4

(d) Soft spring, coupling point at waveguide 1 of MS

(e) Soft spring, coupling point at waveguide 3 of MS

(f) Hard spring, HS node 2

(g) Hard spring, HS node 3

(h) Hard spring, HS node 4

(i) Hard spring, coupling point at waveguide 1 of MS

(j) Hard spring, coupling point at waveguide 3 of MS

Figure 6: **Transversal accelerance FRFs [m/(s$^2$N)] obtained using the Altair® HyperMesh® 2021 finite element software (——) and our approach (- - -), considering soft and hard coupling springs.**

An important question related to the presented analysis is the following: since $n_b = 14$, why 14 wave modes were not used for the WFEM wave basis? This is because some eigenvalues become excessively large and others close to zero, which cannot be adequately evaluated due to floating-point arithmetic errors. To tackle this issue, one could consider a coarser unit cell mesh, so it would be possible to compute all wave modes (albeit in a fewer number) related to the referred mesh.

## 4. CONCLUSIONS

In this article, we have discussed modifications that need to be done in the traditional SEM and WFEM equations to take into account couplings which might exist between a HS and a MS, which can be modeled by discrete springs. Developed equations were applied to model the coupling between a clamped-free beam host structure and a very simple periodic structure (in fact, a mere slender beam). Although naive, the considered problem was valuable to validate the proposed procedures. In addition, it allowed one to have insights on possible issues which might harm the combination of WFEM and SEM strategies.

One should also point out that dispersion relations computed for the uncoupled unit cell showed perfect agreement with those obtained using analytical expressions. In addition, the obtained dispersion relations showed that the unit cell dynamics is changed by increasing the coupling stiffness. In the case of soft coupling, cut-on frequencies were evidenced for both longitudinal and bending behaviors. By increasing the coupling stiffness to the hard spring configuration, the cut-on frequency moved beyond the analyzed frequency range, being the longitudinal and/or bending wave modes highly evanescent.

Accelerances FRFs computed by the proposed SEM–WFEM coupled equations showed very good agreement with respect to those obtained through the conventional finite element method. Higher order evanescent modes might not be negligible for certain responses, due to the fact that they can be important for the coupled system dynamics. Also, the use of the CB method deteriorates results provided by the proposed approach, if DOFs of the MS which participate in the coupling become condensed. One still needs to investigate if the CB method is able to provide better results when DOFs of the MS which participate in the coupling are not dynamically reduced.

In our next work, we will assess how the coupling of a true MS (for instance, with bandgaps) to a HS can influence the

dynamic behavior of the latter, using the presented strategy, since one should be able to consider a relatively complex unit cell with the WFEM.

## 5. ACKNOWLEDGMENTS

V. M. S. Santos acknowledges his master scholarship by the Brazilian National Council for Scientific and Technological Development (CNPq). Both authors are grateful to the São Paulo Research Foundation (FAPESP) for its support to the thematic grant #18/15894-0, related to the "Periodic structure design and optimization for enhanced vibroacoustic performance: ENVIBRO" research project.

## 6. REFERENCES

Banerjee, A., Das, R. and Calius, E.P., 2019. "Waves in Structured Mediums or Metamaterials: A Review". *Archives of Computational Methods in Engineering*, Vol. 26, No. 4, pp. 1029–1058. ISSN 1886-1784. doi:10.1007/s11831-018-9268-1.

Doyle, J., 2020. *Wave Propagation in Structures*. Mechanical Engineering Series. Springer International Publishing. ISBN 9783030596798.

Duhamel, D., Mace, B. and Brennan, M., 2006. "Finite element analysis of the vibrations of waveguides and periodic structures". *Journal of Sound and Vibration*, Vol. 294, No. 1-2, pp. 205–220. doi:10.1016/j.jsv.2005.11.014.

He, F., Shi, Z., Qian, D., Tu, J. and Chen, M., 2022. "Flexural wave bandgap properties in metamaterial dual-beam structure". *Physics Letters A*, Vol. 429, p. 127950. doi:10.1016/j.physleta.2022.127950.

Hoang, T., Duhamel, D. and Foret, G., 2020. "Wave finite element method for waveguides and periodic structures subjected to arbitrary loads". *Finite Elements in Analysis and Design*, Vol. 179, p. 103437. doi:10.1016/j.finel.2020.103437.

Hussein, M.I., Leamy, M.J. and Ruzzene, M., 2014. "Dynamics of Phononic Materials and Structures: Historical Origins, Recent Progress, and Future Outlook". *Applied Mechanics Reviews*, Vol. 66, No. 4. ISSN 0003-6900. doi:10.1115/1.4026911.

Lee, U., 2009. *Spectral Element Method in Structural Dynamics*. Wiley. ISBN 9780470823750.

Mencik, J.M., 2014. "New advances in the forced response computation of periodic structures using the wave finite element (WFE) method". *Computational Mechanics*, Vol. 54, No. 3, pp. 789–801. doi:10.1007/s00466-014-1033-1.

Mencik, J.M. and Duhamel, D., 2015. "A wave-based model reduction technique for the description of the dynamic behavior of periodic structures involving arbitrary-shaped substructures and large-sized finite element models". *Finite Elements in Analysis and Design*, Vol. 101, pp. 1–14. doi:10.1016/j.finel.2015.03.003.

Mencik, J.M., 2010. "On the low- and mid-frequency forced response of elastic structures using wave finite elements with one-dimensional propagation". *Computers and Structures*, Vol. 88, pp. 674–689. doi:10.1016/j.compstruc.2010.02.006.

Mencik, J.M., 2018. "A wave finite element approach for the analysis of periodic structures with cyclic symmetry in dynamic substructuring". *Journal of Sound and Vibration*, Vol. 431, pp. 441–457. doi:10.1016/j.jsv.2018.05.027.

Mizukami, K., Funaba, K. and Ogi, K., 2021. "Design and three-dimensional printing of carbon-fiber-composite elastic metamaterials with inertial amplification mechanisms". *Journal of Sound and Vibration*, Vol. 513, p. 116412. doi:10.1016/j.jsv.2021.116412.

Muhammad and Lim, C.W., 2022. "From Photonic Crystals to Seismic Metamaterials: A Review via Phononic Crystals and Acoustic Metamaterials". *Archives of Computational Methods in Engineering*, Vol. 29, No. 2, pp. 1137–1198. ISSN 1886-1784. doi:10.1007/s11831-021-09612-8.

Silva, P.B., Mencik, J.M. and de França Arruda, J.R., 2016. "Wave finite element-based superelements for forced response analysis of coupled systems via dynamic substructuring". *International Journal for Numerical Methods in Engineering*, Vol. 107, No. 6, pp. 453–476. ISSN 1097-0207. doi:10.1002/nme.5176.

Vivien, D. and Mencik, J.M., 2020. "A wave-based optimization approach of curved joints for improved defect detection in waveguide assemblies". *Journal of Sound and Vibration*, Vol. 465, p. 115003. ISSN 0022-460X. doi:10.1016/j.jsv.2019.115003.

Waki, Y., Mace, B. and Brennan, M., 2009a. "Free and forced vibrations of a tyre using a wave/finite element approach". *Journal of Sound and Vibration*, Vol. 323, No. 3-5, pp. 737–756. doi:10.1016/j.jsv.2009.01.006.

Waki, Y., Mace, B. and Brennan, M., 2009b. "Numerical issues concerning the wave and finite element method for free and forced vibrations of waveguides". *Journal of Sound and Vibration*, Vol. 327, No. 1-2, pp. 92–108. doi:10.1016/j.jsv.2009.06.005.

Zhong, W. and Williams, F., 1995. "On the direct solution of wave propagation for repetitive structures". *Journal of Sound and Vibration*, Vol. 181, No. 3, pp. 485–501. doi:10.1006/jsvi.1995.0153.

Zhou, C.W., Lainé, J.P., Ichchou, M.N. and Zine, A.M., 2015. "Wave finite element method based on reduced model for one-dimensional periodic structures". *International Journal of Applied Mechanics*, Vol. 07, No. 02, p. 1550018. doi:10.1142/s1758825115500180.

## 7. RESPONSIBILITY NOTICE

The authors are solely responsible for the printed material included in this paper.